Photocatalytic process in TiO2/graphene hybrid materials. Evidence of charge separation by electron transfer from reduced graphene oxide to TiO2

(Article begins on next page)

08 November 2024

The publisher's version is available at:
http://linkinghub.elsevier.com/retrieve/pii/S0920586116302206

When citing, please refer to the published version.

Link to this full text:
http://hdl.handle.net/2318/1622251

iris - AperTO

University of Turin's Institutional Research Information System and Open Access Institutional Repository

Photocatalytic process in TiO$_2$/graphene hybrid materials. Evidence of charge separation by electron transfer from Reduced Graphene Oxide to TiO$_2$

M. Minella, F. Sordello, C. Minero *

Department of Chemistry and NIS Center of Excellence, University of Torino, Via P. Giuria 5, Torino 10125, Italy, http://www.environmentalchemistry.unito.it.
* Corresponding author. Fax +39-011-6705242; E-mail: claudio.minero@unito.it.

Abstract

Different amounts of graphene oxide were chemically reduced with hydrazine in the presence of nanometric TiO$_2$ and SiO$_2$. The photocatalytic performance of the resulting hybrid materials was compared with pristine supports using phenol and methylene blue (MB) under two different irradiation conditions (UV-Vis and Vis only light). MB is strongly adsorbed on the hybrid materials. Significant MB degradation rates were observed on pristine TiO$_2$ and hybrid TiO$_2$-reduced graphene oxide (rGO) material under both irradiation conditions. In the presence of the hybrid catalyst, the degradation of MB under Vis is due to the dye-sensitized mechanism, while under UV-Vis there is an additional semiconductor-based photocatalytic mechanism. Conversely, the presence of rGO reduces the rate of photocatalytic transformation for the poorly adsorbed phenol under UV irradiation, and a negligible degradation rate was observed under Vis.

The UV-Vis absorption spectra of aqueous suspensions of hybrid materials with different rGO loading indicate a strong interaction of the two materials and a reduction of the light absorption due to the presence of rGO. Among many mechanisms reported on the role of rGO, it is inferred that the working mechanism involves electron transfer from photoexcited states of rGO onto the titania, and holes migration from titania to rGO, where adsorbed substrates are oxidized. This oxidation is possible only if the substrate HOMO has higher energy (less positive standard redox potential) than the empty states of excited rGO, supposedly for MB and not for phenol. Then, reduced graphene is advantageous when substrates are adsorbed and when the charge separation is possible (coupled with a proper semiconductor like TiO$_2$). Alone, or coupled with low work function oxides like SiO$_2$, rGO could be ineffective.

Keywords

1. Introduction

The study of the semiconductor/electrolyte and semiconductor/gas interfaces has been driven by their potential multisectorial applications [1,2,3,4,5,6]. The main limits to the application of the related technology are: i) the low photonic efficiency of current photocatalysts; ii) the low absorption in the visible spectrum. Crucial issues are the low efficiency in the photogenerated charge carrier separation and the low rate of interfacial charge transfer reactions. [7] Complex strategies have been proposed to increase the performance of semiconductor photocatalysts [8,9,10,11,12,13,14,15,16,17]. More recently, the enhancement of photocatalytic performances has been obtained with nano-hybrid materials made with semiconductors and carbonaceous structures (fullerenes, carbon nanotubes, carbon nanohorns, and graphene). [18,19,20,21]

The interest in the TiO_2-graphene nano-composites is based on the role that the carbonaceous phase plays in the photocatalytic process. Graphene shows exceptional adsorption ability toward various classes of compounds promoting the adsorption of pollutants on the catalyst surface, prerequisite for their efficient photocatalytic removal if and only if the photogenerated charges move toward graphene.

The methods for the graphene production are numerous [22,23,24,25], but the synthesis of non-functionalized graphene does not allow the production of TiO_2-graphene hybrid materials due to the absence of functional groups able to bond to the semiconductor [26,27]. For these reasons the most useful method for the synthesis of TiO_2-graphene photocatalysts is based on the synthesis of graphite oxide by means of chemical oxidation, its exfoliation in water and subsequent reduction of graphene oxide (GO). The final materials are usually defined as reduced GO (rGO), whatever the reduction strategies are, due to the partial preservation of some oxidized moieties in their structure. [28,29]

In the degradation of organic substrate on TiO_2-rGO composites, the main active oxidation species were inferred from the disappearance kinetics of different substrates in the presence of $^\bullet OH$ and hole (h_{vb}) scavengers. These experiments demonstrated that the main reactive species are not free hydroxyl radicals and that the direct hole transfer is the main mechanism. [30,31]

Till now a complete agreement on the role of rGO during the photocatalytic process on TiO_2-rGO hybrids has not be reached. The operational mechanisms active on TiO_2-rGO composites as emerges from literature can be summarized as follow.

    A. In the case of substrates that do not absorb light and are negligibly adsorbed on catalyst the photodegradation could take place mainly via the "classic" UV-based photocatalytic process promoted by UV-activated band to band transition in which no electron transfer between TiO_2 and rGO is operational and rGO acts only as competitive light absorber, because the GO and rGO electronic structure could preclude any injection of electrons from TiO_2 toward the carbonaceous phase or *vice-versa*. [30]. In addition, the adsorption of carbonaceous phase can generate intraband gap states, located immediately above the VB or below the CB which can extend the absorption of light to the Vis range.

    B. When the movement of photogenerated charges from the two phases (TiO_2 and rGO) is not hindered and substrates which do not absorb light are involved, two possible and alternative mechanisms can operate.

1) Electron transfer from rGO to TiO_2. The photocatalytic process is promoted by rGO, which absorbs visible (and UV) photons. Photo-excited electrons in high-energy rGO states are then delocalized (with kinetics in the 0.1-0.2 ps range [32]) onto the TiO_2 structure. Zhang and co-workers demonstrated the role of graphene as a macromolecular photosensitizer instead of an electron reservoir on irradiated rGO-ZnS composites. [33] The time-domain *ab initio* analysis carried out by Long and co-workers [32] highlighted that electron transfer process can occur from photoexcited states of perfect graphene sheets onto the titania surface with a non adiabatic

2

89   mechanism. The injected electron located in interfacial states then moves into bulk TiO_2
90   dissipating the energy *surplus* due to electron-vibrational interactions. [32]

91   2) Electron transfer from TiO_2 to rGO. A UV-based transaction promotes electrons into the
92   TiO_2 CB which are rapidly transferred onto the graphene-like sheets. The common reaction
93   scheme proposed for the interface rGO/TiO_2 allows the delocalization of TiO_2 CB electrons onto
94   the rGO structure (rGO in this case acts as an electron reservoir). The work function of graphene
95   is 4.42 eV, while the conduction band (CB) of TiO_2 is located at –4.21 eV with energy gap
96   amplitude of 3.2 eV (for the most photoactive anatase allotrope). [34,35,36] As a consequence,
97   the electrons photo-promoted in the CB can be injected into the graphene aromatic structure
98   avoiding their recombination with the valence band (VB) holes. The decrement of the electron
99   transfer resistance at the TiO_2-rGO/electrolyte interface compared to that at the TiO_2/electrolyte
100   interface, observed with EIS by Wang et al., suggested a rapid photoinduced charge separation
101   and a diminished possibility of electron–hole recombination on irradiated TiO_2-rGO materials.
102   [31] Wang et al. proposed that not only electrons can be easily transferred from photo-excited
103   TiO_2 onto rGO sheets, but also valence holes can move toward the rGO phase promoting an
104   effective degradation of adsorbed phenol molecules. [37]

106   The injection of electrons from excited rGO states toward TiO_2 CB or alternatively from TiO_2
107   CB toward delocalized empty rGO states is not a sufficient condition to guarantee the
108   degradation of the substrate, because the photogenerated empty states (a hole in the VB or an
109   empty states in the rGO) must be low enough in energy (redox potential sufficiently positive) to
110   promote the oxidation of the substrate itself (injection of an electron from the substrate to the
111   photogenerated empty state). It is worth noting the stability of certain organic substrates under
112   UV irradiated TiO_2 as a consequence of their too low HOMO energetic position (e.g. cyanuric
113   acid is stable in photocatalytic conditions [38,39]). Consequently, the energetic position of the
114   HOMO of a substrate is a key point to allow its transformation under irradiated TiO_2-rGO
115   hybrids especially in the case of Vis only irradiation which does not activate TiO_2 band to band
116   transitions which generate very oxidant VB holes.

118   C.   In the presence of dyes, other two different visible-activated dye-sensitized pathways
119   have to be considered: in the case of a pure TiO_2 catalyst the adsorbed dyes can inject
120   photo-excited electrons onto the titania CB, while in the presence of TiO_2-rGO
121   composites this mechanism can couple with an alternative reaction path in which the dye
122   photo-excited electrons can be delocalized in the electronic diffuse states of rGO. In both
123   cases the oxidized dye molecules, formed as a consequence of a single or multi-electron
124   injection from the photo-excited dye to the delocalized empty states of rGO or TiO_2, can
125   autonomously evolve toward transients or stable by-products and consequently toward
126   the substrate degradation. Pastrana-Martínez et al. from an in depth analysis of the
127   photocatalytic activity of TiO_2-rGO composites toward the colorless diphenhydramine
128   and the organic dye methyl orange, emphasized the complexity of the operational
129   mechanisms concluding that rGO can operate as visible light sensitizer of TiO_2, but in the
130   presence of visible-absorbing species the degradation process can be dominated by a
131   direct self-oxidation of the visible-absorbing species. [30]

133   Herein, we report the two-steps synthesis of TiO_2-rGO hybrid materials (synthesis of GO by
134   chemical oxidation of graphite, exfoliation and in situ reduction of GO on the TiO_2 surface) and
135   the investigation of their photocatalytic behavior. The photocatalytic tests were carried out
136   comparing two substrates and two illumination sources aiming to give insight on the working
137   mechanisms and on the relation between the absorbing optical properties of the tested catalyst
138   and its photocatalytic behavior. This approach allows us to discriminate among the potential

3

139 operational photocatalytic mechanisms cited above and, hopefully, to clarify some aspects of the
140 photo-reactivity of TiO_2-rGO composites.

2. Materials and Methods

2.1 Materials

143 Graphite natural powder (briquetting grade, $\approx$ 100 mesh, 99.9995%) was purchased from Alfa
144 Aesar, H_3PO_4 (85%), H_2SO_4 (96%), $KMnO_4$ (>99%), HCl (37%), methanol gradient grade from
145 Carlo Erba and $HClO_4$ (85%), Methylene Blue (MB) trihydrate (>99%), H_2O_2 (35%), hydrazine
146 monohydrate (98%) and phenol (>99%) from Sigma Aldrich. Titanium dioxide (Hombikat
147 N100: 100% anatase, BET specific surface area 100 m^2/g, average crystal size 20 nm) was
148 purchased from Sachtleben Pigments. Fumed silica SiO_2 Aerosil OX 50 (BET specific surface
149 area 50 m^2 g^{-1}) was bought from Evonik. Zero-grade air for Total Organic Carbon (TOC)
150 analysis was purchased from Sapio (Turin, Italy). All the compounds were used as received
151 without any further purification step. Water was purified with a MilliQ plus apparatus (in-line
152 TOC = 2 ppb, conductivity 18.2 MΩ cm, Merck Millipore).

2.2 Synthesis of GO and TiO_2-rGO hybrid materials

154 Graphene oxide was produced by chemical oxidation using the modified Hummers and
155 Staudemaier's method [40] proposed by Huang et al. [41]. Briefly, 500 mg of graphite powder
156 were dispersed in a solution obtained with 27.3 mL H_2SO_4, 3.30 mL H_3PO_4 and 2.78 g $KMnO_4$.
157 The suspension was magnetically stirred at r.t. for 1, 2 or 3 days, respectively. After 12-15 hours
158 a viscous brownish gel was obtained. After the desired oxidation time the suspension was
159 carefully diluted in 120 mL of water and titrated with H_2O_2 till a bright yellow suspension was
160 obtained (the violet MnO_4^- ions are completely reduced to colorless Mn^{+2}). The yellow graphite
161 oxide formed was washed three times with 1 M HCl and the solid separated with centrifugation
162 (1200 G). During the washing procedure the color changed from bright yellow to brownish. The
163 solid was then washed 3 times with water. During the washing procedure the graphite oxide
164 experienced exfoliation. The suspension was then dialyzed toward water (Spectra/Por® Dialysis
165 Membrane, MW cut off 6-8000 Da) until the pH of the external solution was stable and close to
166 4. The concentration of carbon in the GO suspensions was evaluated measuring the TOC on
167 diluted suspensions after dialysis.
168 The TiO_2-rGO hybrid materials were obtained by chemical reduction with hydrazine solution
169 (65 %) of different amounts of GO (3 days of oxidation) in the presence of TiO_2 according to a
170 modification of the method reported in [42]. Stable suspensions of 4 g dm^{-3} TiO_2 in water were
171 obtained by sonication. Different amounts of GO were added to obtain materials with different
172 carbon loading. The addition of GO quickly destabilized the TiO_2 colloids owing to adsorption
173 of GO on the titania surface. Then 300 μL of hydrazine were added drop wise at r.t. After 12
174 hours of vigorous stirring the suspensions were filtered on 0.45 μm hydrophilic filters
175 (Whatman, NL 17 membrane filters, polyamide) and washed with water. Finally, the produced
176 powder was dried at 373 K for 1 hour.
177 By using the same method adopted for the synthesis of TiO_2-rGO materials, we produced
178 hybrid SiO_2-rGO materials with different loading of rGO. GO was adsorbed on fumed silica
179 SiO_2 Aerosil OX 50 and reduced with hydrazine. The synthesis of these hybrid materials was
180 aimed to study the photochemical behavior of the rGO adsorbed on an inert support. The low
181 work function of SiO_2 ($\chi \approx$ 1.2 eV [43]) hinders the injection of electrons from the excited states
182 of rGO to the inorganic support allowing the study of the photochemical behavior of rGO alone.

4

2.3 Photocatalytic Tests

The photodegradation experiments were carried out using cylindrical Pyrex cells (4.0 cm diameter and 2.5 cm height, cut-off at 295 nm) on 5 cm^3 of aqueous suspension containing the desired amount of the photocatalyst powder (C_{cat} 0.5 g dm^{-3}), substrate (1 mM phenol or 4×10^{-5} M MB) and HClO$_4$ 10^{-3} M to execute the test at pH 3±0.2. The slurries containing the photocatalyst were prepared using sonication. The irradiation was carried out with a set of three TLK 40W/05 (UV-Vis) or TLK 40W/03 (Vis only) fluorescent lamps (Phillips, Eindhoven, Nederland). The former has an integrated irradiance of 25.2±1 W m^{-2} in the 300-400 nm wavelength range, with a maximum emission at 365 nm (able to activate the band to band transition in TiO$_2$ based materials), and minor emission in the Vis range (10.5±1 W m^{-2} in the 400-800 nm range). The latter has an integrated irradiance of 40±1 W m^{-2} in the 400-800 nm wavelength range, with a maximum emission at 423-436 nm, and negligible emission in the UV range (1.5 W m^{-2} in the 300-400 nm range). The emission spectra are reported in Fig.1A of the Supplementary Materials (hereafter SM).

During irradiation the suspension was magnetically stirred and the cell temperature was 30±3 °C. After irradiation the suspension was filtered through 0.45 μm cellulose acetate membrane filter (Millipore HA) and analysed as required (HPLC-UV for phenol, spectrophotometrically at 665 nm for MB).

The photocatalytic transformation of the studied substrates followed pseudo-first order kinetics. The profiles of concentrations of the phenol and MB were fitted with a pseudo-first order equation of the form $C_t / C_0 = \exp(-k\, t_{irr})$, where C_t is the substrate concentration at the irradiation time t_{irr}, C_0 the initial concentration, and k the pseudo-first order degradation rate constant. The values of k are reported with their uncertainty (confidence intervals evaluated through the goodness of the fit, representing intra-series variability at 0.95 level of confidence).

2.4 Methods

The extinction spectra of TiO$_2$, TiO$_2$-rGO, SiO$_2$ and SiO$_2$-rGO suspensions were recorded with a Varian CARY 100 Scan UV-Vis spectrophotometer, using quartz cuvettes with a path length of 1 cm. The % reflectance spectra were recorded on opaque homogenized powdered samples with a Varian Cary 5000 UV-VIS-NIR reflectance spectrometer.

The UV-Vis lamp irradiances were measured with an Ocean Optics USB2000+UV-VIS equipped with a 400 μm optical fiber (30 cm length) with a cosine corrector (Ocean Optics, CC-3-UV-T, optical diffuser in PTFE, wavelength range 200-2500 nm, OD diameter 6.35 mm, Field of View 180°). The spectrometer was calibrated with an Ocean Optics DH-2000-CAL Deuterium-Halogen Light Sources for the UV-Vis-NIR calibrated for absolute irradiance measurements from the vendor (Radiometric Calibration Standard UV-NIR, certificate of calibration #2162).

Phenol degradation kinetic was monitored with HPLC-UV (Hitachi L2200, LaChrom Elite, Lichrospher R100-CH 18/2 column (250 mm)). The elution was carried out at 1 cm^3 min^{-1} with H$_3$PO$_4$ 4.2 mM: Methanol 85:15 in isocratic mode. The retention time of phenol under this condition is 9.9 minutes. The injection volume was 60 μL.

The measurement of TOC was carried out with a Shimadzu TOC-VCSH Total Organic Carbon Analyzer, equipped with an ASI-V autosampler and fed with zero-grade air. Each suspension of GO, as synthesized, was diluted 200 times with MQ water and analyzed. TOC was obtained from the difference between Total Carbon (TC) and Inorganic Carbon (IC).

The morphology of the hybrid samples before (TiO$_2$-GO) and after the reduction with hydrazine (TiO$_2$-rGO) was investigated by means of a high-resolution transmission electron microscope (HR-TEM, JEOL JEM 3010), equipped with a LaB$_6$ source with an accelerating voltage of 300 kV.

5

232 The XPS analysis was carried to investigate the nature of the carbon atoms in the TiO_2-GO and
233 TiO_2-rGO samples. The XPS spectra were recorded on pelletized samples with a VSW TA10 Mg
234 Kα X-ray source (1253.6 eV) equipped with a VSW Class 100 Concentric Hemispherical
235 Analyzer (VSW Scientific Instruments Ltd).
236

# 3 Results and Discussion

3.1 Material characterization

239 The simple oxidation method here adopted allows the preparation of significant amount of GO,
240 the raw material for the successive synthesis of rGO, contrariwise to the sonochemical methods
241 adopted for the exfoliation of graphite and one-step production of micro-amount of graphene
242 nanosheets. [23,44,45]
243 Fig. 1 shows the UV-Vis absorption spectra of the suspensions of GO obtained after 1, 2 and 3
244 days of chemical oxidation, respectively. The spectra are normalized for the TOC concentration
245 of the analyzed suspensions. The spectra are dominated by the peaks at ≈230 nm. These signals
246 are due to the $\pi \rightarrow \pi^*$ transition of the C=C bonding. [41,46,47] The accurate position of the
247 peaks are 231, 229 and 228 nm for the samples oxidized for 1, 2 and 3 days (*1D*, *2Ds*, *3Ds*),
248 respectively. The lower is the peak position (as wavelength) the lower is the degree of
249 aromaticity of the graphene-like planar structure. Accordingly, the *3Ds* sample shows the peak at
250 the shortest wavelength. The main peaks has a shoulder at roughly 300 nm, due to the $n \rightarrow \pi^*$
251 transition of the carbonyl groups. [48,49] The larger is the intensity of the 300 nm shoulder, the
252 larger is the concentration of C=O (carbonyl or carboxyl) groups in the samples and so the
253 degree of oxidation. The ratio between the absorbance at 230 and 300 nm is also informative.
254 This ratio is 2.4, 2.6 and 2.8 for the *1D*, *2Ds* and *3Ds* samples, respectively. It increases with the
255 increment of the oxidation degree because superior is the oxidation of graphene basal planes,
256 greater it is the amount of isolated aromatic rings which increment the absorbance at 230 nm
257 [49]. The obtained ratios (> 2) are very similar to those reported by Huang et al. [41] for GO
258 samples with significantly larger lateral size.
259 The size of the GO particles after three days of oxidation in the same condition above
260 described has been previously measured with dynamic light scattering (DLS) and reported in
261 [29]. After exfoliation the GO particles have a hydrodynamic radius equal to 500 ± 70 nm. This
262 value is in agreement with those reported by other authors for GO obtained in very similar
263 experimental conditions [50].
264 The proposed methods for the reduction of GO to graphene are numerous (thermal annealing,
265 microwave and photo reduction [29], chemical, photocatalytic and solvothermal reduction) and
266 affect the final performance of materials. For a full analysis of this topic please refer to the
267 review by Pei and Cheng [51]. The production of the TiO_2-rGO was here carried out by chemical
268 reduction of different amount of GO (*3Ds*) adsorbed on the TiO_2 surface with aqueous hydrazine
269 solution. Different materials with increasing amount of carbon loading (from 0.5 to 5% w/w)
270 were successfully synthesized. The chemical reduction in water by hydrazine and its derivatives
271 results in agglomerated graphene-based nanosheets due to the increase of hydrophobicity. [37]
272 We carried out the reduction of GO adsorbed on TiO_2 at r.t. and at the boiling point. We
273 observed that only in the former case is a single solid phase synthesized, while in the latter case
274 two separated phases are produced. Gao et al. [49] studied systematically the reduction of GO by
275 hydrazine at r.t. and at high temperature. The hydrazine reduction at r.t. completely reduces the
276 epoxide and hydroxyl groups located at the interior of the aromatic domains and only partially
277 the carboxyl moieties at the edge of the aromatic domains. At higher temperature the reduction
278 of the hydroxyls at the edge of the aromatic domains and of the carboxyl groups occurs. [49] Our
279 experimental results support the conclusion that heating allows further reduction of the

6

280 oxygenated groups which links GO to the TiO$_2$ surface (e.g. the ester groups obtained from the
281 reaction between the TiO$_2$ hydroxyls and the carboxyls of GO). Furthermore, the increment of
282 the hydrophobicity of rGO at higher reduction temperature hinders the interaction between rGO
283 and the hydrophilic TiO$_2$ surface causing phase separation. Thus, the materials used for the
284 photocatalytic tests are those obtained by reduction at r.t. only.

285
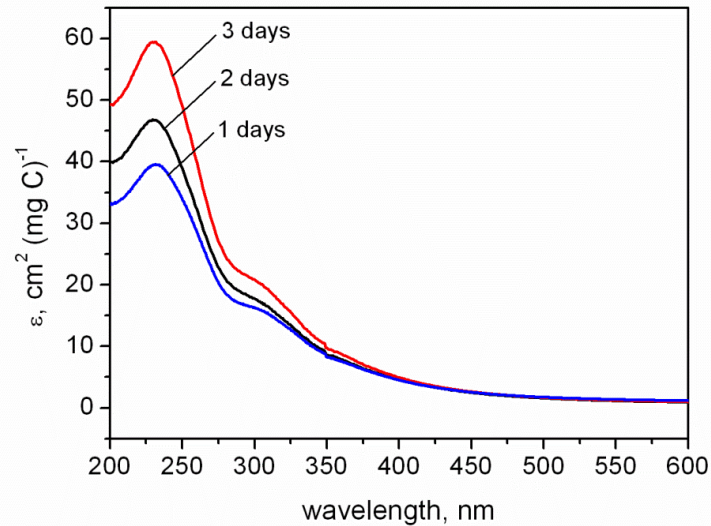
286 **Fig. 1** Absorption spectra of graphene oxide colloid (GO) obtained after different oxidation times (1, 2
287 and 3 days). The measured absorbance is normalized for the total organic concentration (TOC) of each
288 measured solution.

289   Fig. 2-SM and Fig. 3-SM show the HR-TEM micrographs of TiO$_2$-GO and TiO$_2$-rGO (both
290 with a 5% carbon loading) at different magnifications. No significant differences were observed
291 before and after the chemical reduction of GO with hydrazine at room temperature. The anatase
292 nanoparticles have an average particle size of $\approx$20 nm and are dispersed on the 2D layers of the
293 graphene structure, which in some cases enfold the TiO$_2$ nanoparticles.
294   The effective reduction with aqueous hydrazine of the GO to rGO was evaluated with XPS-
295 ESCA. Fig. 4-SM shows the spectra of the TiO$_2$-GO and TiO$_2$-rGO (both with a 5% carbon
296 loading) in the C(1s) core level peak region. The spectrum of TiO$_2$-GO is dominated by three
297 main overlapped peaks. The peak centered at $\approx$ 285 eV is related to carbon atoms in sp2
298 hybridization typical of graphitic/graphenic structures, while the components at higher binding
299 energy (BE at $\approx$ 287 and 289 eV) can be attributed to carbon species in higher oxidation state.
300 [52,53 and references therein]. In the case of the reduced sample one peak dominates the spectra
301 (BE at $\approx$ 285), concurrently with a strong suppression of signals for high C-oxidation state. From
302 the comparison of the two spectra (Fig. 4-SM a and b) it is manifest the effective reduction of the
303 carbonaceous phase was obtained with hydrazine.
304   Fig. 5-SM shows the diffuse Reflectance spectra of the produced TiO$_2$-rGO materials in the
305 200-800 nm range, as *%R* and as Kubelka-Munk (K-M) function (eq. 1, left). The rGO phase
306 induces the improved light absorption in the Vis range in line with data previously reported for
307 TiO$_2$-rGO hybrid materials. [54,55,56] The energy band gap values of the synthesized materials
308 were evaluated from the K-M functions by considering the relation which links the ratio between
309 the absorption and scattering coefficients and the photon energy for semiconductors with indirect
310 band gap, e.g. TiO$_2$ (eq. 1, right).

311
$$f(R) = \frac{(1 - R_\infty)^2}{2\,R_\infty} = A\left(h\nu - E_g\right)^2 \qquad\qquad\text{eq. 1}$$

7

where $f(R)$ is the K-M function, R_∞ the diffuse reflectance approaching infinite sample thickness, hv the photon energy, E_g the energy gap and A is a constant.

A slight decrement of the apparent E_g values (from 3.28 to 3.20 eV, corresponding to a red shift from 378 to 387 nm, see the inset of Fig. 5B-SM) was observed with the increase of the rGO loading. This can be a consequence of the production of a limited number of localized intraband gap states or simply an apparent band gap due to the superposition of absorption spectra of two different materials. However the slight decrement of the E_g we observed is negligible if compared to that reported for other TiO_2-carbon phase (graphene, carbon nanotubes) hybrid materials. [55,57,58]

The extinction spectra of water suspensions of the studied catalysts at different concentration (10, 50 and 100 mg dm^{-3}) were recorded and the average extinction coefficient $\varepsilon_{ext}(\lambda)$ (Fig. 2A) computed from the plot of absorbance vs concentration, according to the Beer-Lambert law. The linear fits have r > 0.998 for all the wavelengths. The analysis of the $\varepsilon_{ext}(\lambda)$ values (sum of the absorption, ε_{abs}, and scattering, ε_{scat}, coefficients) reveals that the increment of the rGO loading decreases the intrinsic ability of catalyst suspensions to absorb the radiation in the whole wavelength range, and consequently the overall amount of photons able to activate the UV-based photocatalytic mechanism is diminished. In addition the spectrum of hybrid materials suggests that there is strong interaction between TiO_2 and rGO, as the ratio of typical UV absorption bands of TiO_2 is changed (see bands at 273 and 323 nm, respectively). Moreover a large extinction (absorption + scattering) is present in the Vis range.

Fig. 2B shows the extinction spectra of water suspensions of nanometric silica (average size 40 nm) and of the composite SiO_2-rGO with 1% of carbon loading. The addition of rGO slightly increases the extinction. The spectrum of the SiO_2 colloid, because of the high band gap of silica (8.9 eV [59]), is dominated by the contribution of Mie-scattering only. The SiO_2-rGO colloid retains the scattering profile of silica, overlapped with an almost flat absorption of rGO till 240 nm. Conversely, the rGO loading on TiO_2, which has similar surface hydrophilicity of SiO_2, reduces the UV-Vis extinction and totally changes the absorption spectrum, indicating a strong interaction between rGO and the semiconductor electronic structure. The absorption peak of rGO below 240 nm (Fig. 2B) is also manifest in the spectra of TiO_2-rGO colloids at $\lambda < 240$ nm (Fig. 2A), where this peak overlaps with the complex profile resulting from the scattering and absorption properties of TiO_2 strongly modified by the interaction with rGO.
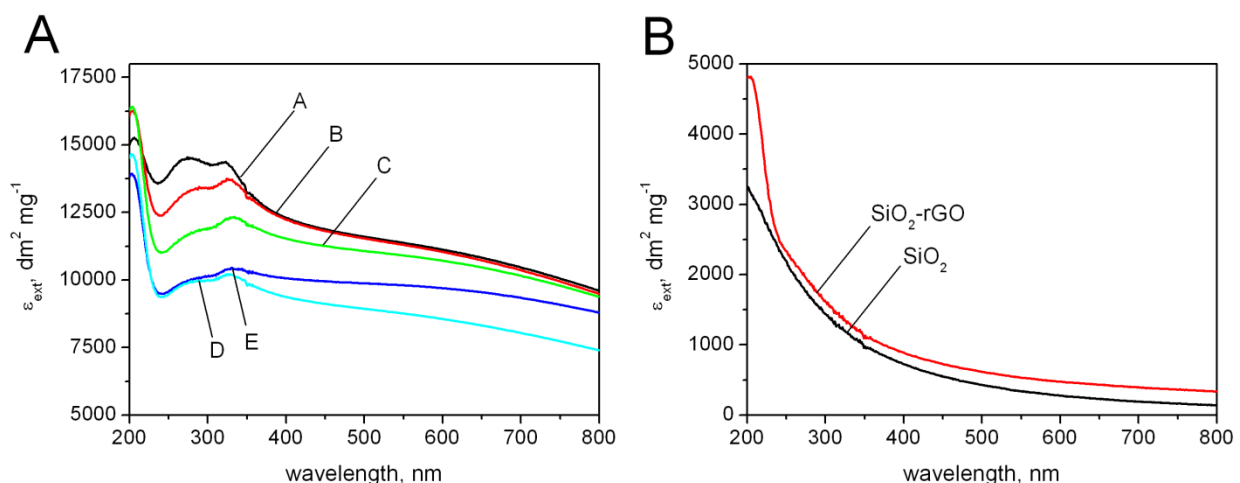

Fig. 2 Extinction coefficient (ε_{ext}) of water suspensions of A) TiO_2-rGO hybrid materials with different % rGO: A= 0 %; B= 0.5 %; C= 1.0 %; D= 2.5 %; E= 5.0 %; B) SiO_2 and SiO_2-rGO (1 % of rGO) The values of ε_{ext} were obtained from the extinction spectra of suspensions with concentrations equal to 10, 50 and 100 mg dm^{-3} of the hybrid material.

8

3.2 Photocatalytic experiments

The photocatalytic performance of the synthesized photocatalysts was evaluated using two different compounds, phenol and MB, under UV-Vis (TLK 40W 05 lamp) and Vis only irradiation (TLK 40W 03 lamp). The absorption spectra of phenol and MB in water solution are reported in Fig.1B-SM. The comparison of lamp emission spectra and substrate absorption spectra (Fig. 1-SM) shows that phenol does not absorb with both lamps, whilst MB absorbs from both lamps the two emission peaks in the 540-580 nm range and from the TLK03 (Vis spectrum) absorbs in the 420-480 nm range in its peak tail.

The MB spectrum in solution changes when MB is adsorbed. Fig. 3 reports reflectance spectra of MB adsorbed on pristine TiO_2 and the MB adsorbed as a function of the solution concentration (KM function, inset of Fig. 3). To measure the spectra, definite amounts of pristine TiO_2 were equilibrated in the dark in the presence of increasing amount of MB (0 to 8.0×10^{-5} mol/g TiO_2). After equilibration the suspensions were filtered and dried in oven at 373 K for 1 hour. The dried powders were grinded and their %R spectra were recorded. As Fig. 3 reports, the quantity adsorbed is linear with MB solution concentration, indicating that at 8.0×10^{-5} mol g^{-1} on pristine TiO_2 the surface is far from saturation of the MB adsorbing sites. The same ratio $[MB]/C_{TiO_2}$ will be used during the photodegradation experiments. From reflectance spectra of Fig. 3 it is also manifest a blue shift of ≈ 80 nm for the MB absorption maximum. This shift is comparable to that reported in the literature [60,61,62] for the formation of MB dimers. Because the significant adsorption of MB onto the TiO_2 surface, the blue shift can be ascribed to adsorption on TiO_2 surface. A shift of ≈ 80 nm of the absorption maximum corresponds to a transition between two states separated by 0.24 eV in energy, and an equilibrium adsorption constant of roughly 1.2×10^4, slightly larger than the reported values ($3-10\times10^3$) for dimerization in solution [60,61,62]. The strong interaction of MB with the catalyst surface is an essential condition for an efficient electron transfer in the case of correct positioning of the energy bands/states. This shift increases the absorption of adsorbed MB in the presence of TLK03 (Vis spectrum), whilst it has only a minor effect on absorption in the case of illumination with the TLK05 (UV spectrum).
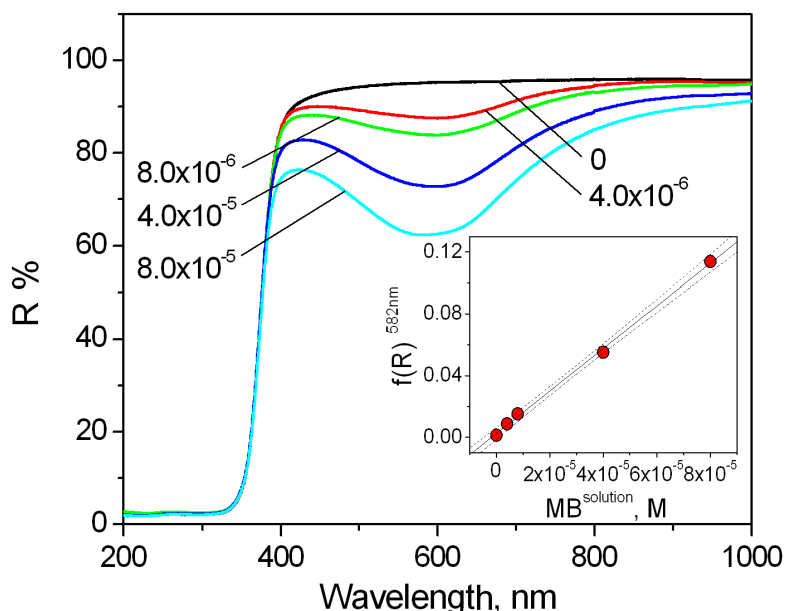
Fig. 3 % Reflectance spectra of TiO_2 Hombikat N100 equilibrated in the presence of different amount of MB (mol MB / g TiO_2 from 0 to 8.0×10^{-5} mol/g). Inset: K-M function value at 582 nm ($f(R)^{582nm}$) for the samples equilibrated at different concentrations of MB in solution.

9

3.2.1   Phenol

Fig. 4 shows the photocatalytic time evolution under UV-Vis light of phenol in the presence of TiO$_2$-rGO, with different rGO loading at total catalyst concentration C_{cat} = 0.5 g dm^{-3}. The degradations follow first order kinetics. The degradation kinetic constants are reported in the inset of Fig. 4 and in Table 1-SM (entries 1-5). The phenol degradation rate decreases with the increment of the rGO loading. Opposite to the reported data, where the coexistence of rGO and TiO$_2$ phases induced generally better photocatalytic performances [21,37], in this case the presence of rGO decreases the substrate transformation rate. Under the adopted experimental conditions the amount of phenol adsorbed on TiO$_2$ is negligible compared to the fraction remaining in solution, and in the presence of increasing amount of rGO no increment of the adsorbed fraction of phenol was observed. This evidence is contrasting with data reported by Wang et al. [37] who observed an increment of the adsorbed phenol fraction with the increment of %rGO on TiO$_2$-rGO composites synthesized by a one-step hydrothermal method. The different results could be related to the different synthetic procedure, which could give materials with a significantly different degree of rGO reduction.

As under UV-Vis irradiation only the catalyst absorbs light, the decrease of phenol degradation rate with increasing rGO loading depends on the reduction of extinction spectra as % rGO increases, as already discussed with reference to Fig. 2. Factually, less light is absorbed, leading to a reduced charge carrier production and the decrease of the rate. A competition for UV light between the inorganic and rGO phase was also recently proposed by Xiong et al. [63] to justify the experimental evidences observed with BiOIO$_3$-rGO nanocomposites under Vis and UV irradiation. From spectra in Fig. 2 it is not possible to decouple absorption and scattering processes, although reflectance spectra in Fig. 5-SM suggest that absorption is mainly due to band-gap absorption of TiO$_2$. Then the visible tail observed in Fig. 2 is due only to scattering properties of N100 TiO$_2$. In the presence of rGO, less light is absorbed by TiO$_2$ because of the presence of the adsorbed rGO phase increases the scattering over the entire UV-Vis spectrum. Alternatively, a lowering of the quantum yield due to a larger recombination rate due to an increasing amount of rGO on TiO$_2$ can be invoked. In this case instead of being beneficial, rGO would behave as a recombination center. This would happen independently on the substrate, contrary to many positive effects reported in literature and later in this work. Consequently, this last hypothesis is discarded.
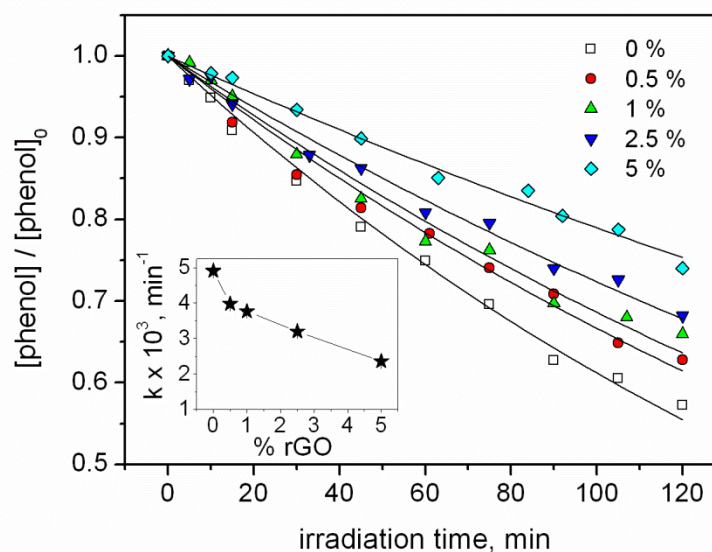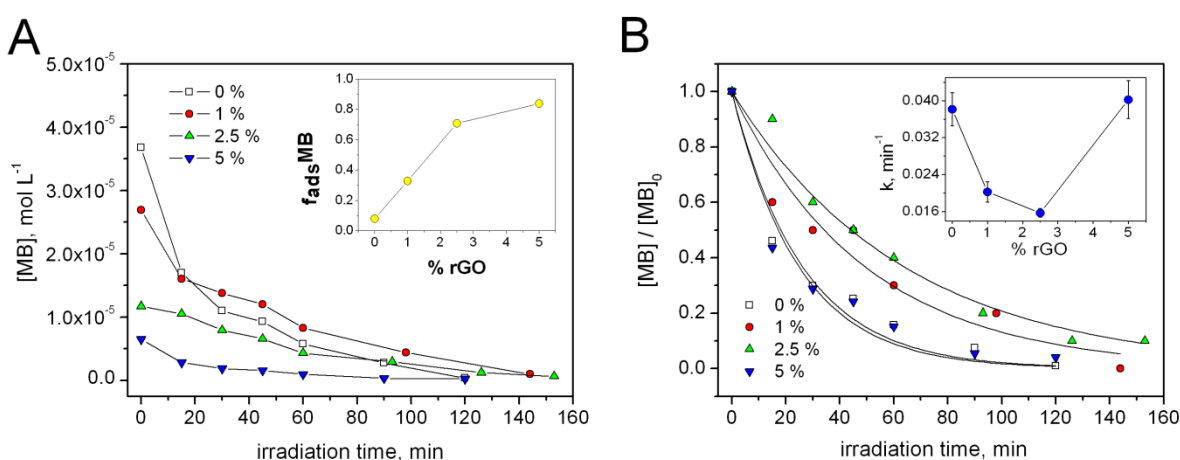

Fig. 4 Photocatalytic degradation under UV irradiation (TLK 40W 05) of 1 mM phenol at pH 3 on TiO$_2$-rGO hybrid materials with different rGO loading. C_{cat} 0.5 g dm^{-3}. Inset: pseudo first order kinetic constants for the photocatalytic transformation of phenol as a function of the % rGO.

10

417   Phenol degradation was also carried out under Vis light (TLK 40W 03 lamp). Very low
418   degradation rates were observed in the presence of both pristine TiO_2 and TiO_2-rGO materials.
419   The kinetic constant observed for TiO_2-2.5% rGO was $(1.9\pm0.1)\times10^{-4}$ min^{-1}, 17 times lower than
420   the degradation kinetic constant measured under UV irradiation. These results indicate that the
421   absorption of the hybrid photocatalyst, and mainly of rGO, as pristine TiO_2 is not excited in the
422   Vis, does not produce photoexcited species able to carry out the reaction with phenol. The
423   possible hypotheses are two: 1) the excited rGO is not able to inject electrons in TiO_2, and
424   photogenerated species recombine in rGO very rapidly compared to their reaction rate with
425   phenol; 2) The excited electrons in high energetic rGO states can be delocalized toward TiO_2
426   conduction band (rGO injects electrons into TiO_2), charge separation is attained and
427   photogenerated species do not recombine, but HOMO of the substrate to be transformed (here
428   phenol) is lower in energy than the energy state of rGO where an electron vacancy has been
429   photogenerated. In this case the reaction is thermodynamically impeded. However it is possible
430   that with other substrates this thermodynamic impediment is removed. As an example, in the
431   case of risperidone, which does not absorb in near UV-Vis, the loading of rGO on TiO_2 increases
432   the photocatalytic rate both under near UV and Vis irradiation.[64]

3.2.2   Methylene Blue

434   Fig. 5A shows the change in the MB concentration under UV-Vis irradiation. The dye
435   concentration in solution before the irradiation is lower than the nominal value in every instance
436   in agreement with the adsorption discussed before (see also Fig. 3) . The adsorption of MB in the
437   adopted conditions is significant and increases with the increment of the rGO loading (e.g. TiO_2-
438   5%rGO adsorbs more than 85 % of the added MB, see inset of Fig. 5A).

439

Fig. 5 Photocatalytic degradation under UV-Vis of 4×10^{-5} M of MB at pH 3 in the presence of TiO_2-rGO
with different % rGO. C_{cat} 0.5 g dm^{-3}. MB concentration (A) and fraction of MB (B) in solution as a
function of the irradiation time. Insets: (A) fraction of MB adsorbed on the catalyst as a function of the %
rGO; (B) pseudo first order kinetic constants for the MB transformation as a function of the % rGO.

445   The C/C_0 showed exponential decay (Fig. 5B). The overall observed kinetic constants k_{obs} are
446   reported as inset in Fig. 5B and in entries 6-9 of Table 1-SM. The observed kinetic constants are
447   deduced from the time evolution of [MB] in aqueous solution as $d[MB_{sol}]/dt=-k_{obs}\times [MB_{sol}]$. The
448   linear relation of $[MB]_{ads}$ vs $[MB]_{sol}$ evidenced in Fig. 3 suggests that $[MB]_{ads} = \beta\ \phi\ C_{cat}\ K$
449    $[MB]_{sol}$, where β is the moles of sites per catalyst mass, ϕ is the fraction of constituent of the
450   hybrid catalyst, C_{cat} is the mass dm^{-3} of hybrid catalyst, and K is the equilibrium adsorption
451   constant. In the case of linear partition between the aqueous phase and rGO / TiO_2 phases, it can
452   be demonstrated that $k_{obs}=k_{tot}$, where k_{tot} is the first order kinetic constant that would be obtained
453   following the time evolution of the total concentration in the system (both adsorbed and free)

454 from $d[MB_{tot}]/dt=-k_{tot}\times[MB_{tot}]$. In other cases they are proportional. Then, the trend of observed
455 kinetic constants k are representative of the overall degradation of substrate in the hybrid system.
456 The rate equations that can be derived from a kinetic model by taking into account the adsorption
457 constants and kinetic constants specific for the two adsorbing phases (k_G and k_T, for rGO and
458 TiO$_2$, respectively), are not developed here as they are outside of the scope of the paper.
459 However, assuming that the rate at the surface is proportional to the local (adsorbed)
460 concentration it can be easily demonstrated that there is no minimum or maximum of k_{obs} as a
461 function of the rGO amount. When $k_G>k_T$, the rate increases with graphene content and vice
462 versa, irrespective of the value of the adsorption constants. Then the observed effects must be
463 explained with factors other than those above cited (adsorption constants and kinetic constants
464 specific for the two adsorbing phases).
465 As observed for the UV photocatalytic abatement of phenol, also in this case the presence of
466 rGO has an initial negative effect. The kinetic constants show a minimum for 2.5% rGO. This is
467 conflicting with the previously reported bell-shaped profile of the rate with the increment of
468 %rGO. [31] The discrepancies point out the role of the method of synthesis which can
469 significantly affect the properties of the material and consequently its photocatalytic behavior.
470 The observed dependence of the rate on the rGO amount can be explained invoking two different
471 effects. At low rGO loading the shielding of TiO$_2$, as already discussed for phenol, decreases the
472 light absorbed by TiO$_2$. In addition, assuming that the reactivity is mainly dominated by TiO$_2$, a
473 stronger adsorption on graphene than on TiO$_2$ implies that the substrate is scarcely transferred
474 during the photocatalytic reaction to the TiO$_2$ surface. It is apparent that because the substrate is
475 adsorbed on graphene, it must react on its surface. Consequently, due to the two cited reasons the
476 overall reaction rate will be reduced unless holes on TiO$_2$ (already decreased by light shielding)
477 are transferred to rGO. As a further increase of rGO loading increases both the MB adsorbed on
478 rGO and the rate, it must definitely concluded that MB reacts on rGO and transfer of holes from
479 TiO$_2$ to rGO is operating. This conclusion agrees with Wang et al. [31] that holes are the main
480 oxidant species and that in the hybrid catalyst oxidative species are not changed by introduction
481 of graphene-like carbon to TiO$_2$. Concurrently with TiO$_2$ excitation, also rGO absorbs light and
482 excited electrons in high energetic rGO states must be delocalized toward TiO$_2$ conduction band
483 (rGO injects electrons into TiO$_2$) to avoid recombination.
484
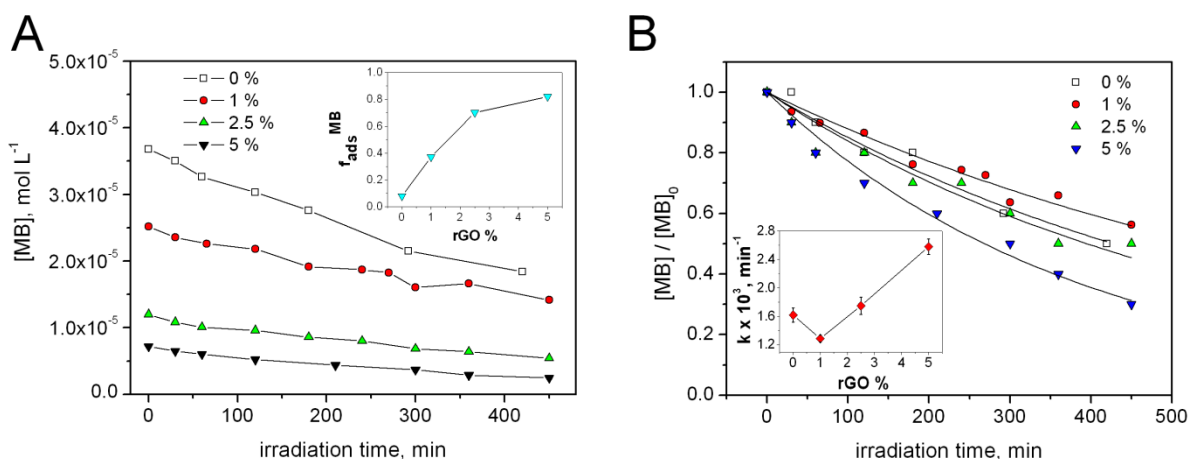
Fig. 6 Photocatalytic degradation under Vis irradiation of 4×10^{-5} M of MB at pH 3 in the presence of TiO$_2$-rGO with different % rGO. C$_{cat}$ 0.5 g dm^{-3}. MB concentration (A) and fraction of MB (B) in solution as a function of the irradiation time. Insets: (A) fraction of MB adsorbed on the catalyst as a function of the % rGO; (B) pseudo first order kinetic constants for the MB transformation as a function of the % rGO.

490 Fig. 6A and Fig. 6B show the change in the MB concentration in solution under Vis irradiation
491 and the related C/C_0 profiles. The amount of MB adsorbed in this experiment (inset of Fig. 6A)

12

492 is quite similar to that observed for previous experiments (inset of Fig. 5A), so a strong
493 adsorption of MB with increasing rGO loading is confirmed. Opposite to the case of phenol
494 photocatalytic degradation under Vis irradiation where negligible removal of the substrate was
495 detected, in this case the MB disappearance is significant, although at irradiation times longer
496 than under UV-Vis irradiation. The abatement profiles follow an exponential decay and the
497 overall k kinetic constants are reported in the inset of Fig. 6B (and entries 10-13 of Table 1-SM).

498 The kinetic constants, after a minimum for TiO_2-1%rGO, increase with the increment of the
499 %rGO, with a shape similar to that observed under UV-Vis irradiation, but with values lower of
500 about one order of magnitude. Under Vis irradiation both rGO and MB can absorb, whilst TiO_2
501 does (almost) not. The slight decrease of the rate at TiO_2-1%rGO could be due to the previous
502 invoked effect of light shielding on TiO_2, as also with the Vis lamp a small absorption by TiO_2 is
503 still possible and a minimal contribution of semiconductor mechanism is present. So the
504 degradation mechanism must involve the light absorption by rGO, or a dye sensitized
505 mechanism.

506 Between the two hypotheses made for justifying the very scarce reactivity of phenol, the first
507 one (fast recombination of photogenerated species in rGO because the excited rGO is not able to
508 inject electrons into TiO_2) must be rejected as MB transforms. The second hypothesis (rGO
509 injects electrons into TiO_2) could be fine if the HOMO of MB is higher in energy than the energy
510 state of rGO where an electron vacancy has been photogenerated. In this case the reaction is
511 thermodynamically favored and charge separation is attained. However, the increase of rGO
512 content implies that the amount of absorbed light is reduced (see Fig. 2A) and consequently the
513 rate would be diminished, contrary to what is observed (inset of Fig. 6B). Then, the MB
514 degradation must be explained by considering a dye-sensitized mechanism.

515 The dye-sensitized mechanism involves the light absorption by MB, charge injection into TiO_2
516 or rGO and evolution of the oxidized MB to products. The absorption of light from the MB-TiO_2
517 surface species was well studied [21,65,66] and the role of self-induced photosensitization
518 outlined.[67] The excited electrons, which occupy the LUMO of the adsorbed MB on TiO_2, can
519 be injected into titania CB promoting the MB degradation. As MB is adsorbed on TiO_2 (Fig. 3)
520 but preferentially adsorbed on rGO (insets of Fig. 5A and Fig. 6A), the electron must be injected
521 from the LUMO of MB to rGO. Then, according to the conclusions drawn from MB irradiation
522 under UV-Vis lamp, rGO would transfer these electrons to TiO_2.

523 To confirm these conclusions, experiments of MB photodegradation under Vis irradiation was
524 carried out in the presence of the SiO_2-rGO hybrid materials synthesized by using the same
525 methods adopted for producing TiO_2-rGO. Under the adopted experimental conditions (0.5 g
526 dm^{-3} of catalyst, initial MB concentration 4×10^{-5} M, pH 3), the silica adsorbs a significant
527 amount of MB (around 75%) and this value increases with the increment of the % rGO. Both on
528 pristine SiO_2 and on SiO_2-rGO hybrid materials, no MB photocatalytic degradation was observed
529 under the adopted conditions. From an energetic point of view an electron in the LUMO of MB
530 adsorbed on the catalyst surface (SiO_2 or SiO_2-rGO) is not able to move toward the CB of SiO_2.
531 This conclusion was expected for SiO_2 due to its very high work function [43]. Then on SiO_2
532 after light excitation of MB only recombination is possible. In the presence of rGO, as reaction
533 does not proceed and also electron transfer from rGO to SiO_2 is impeded because of the SiO_2
534 high work function, the electron transfer to empty electronic states of rGO must be followed by
535 recombination with oxidized MB, giving a null cycle.

536 Then the mechanism of MB degradation in the presence of the hybrid TiO_2-rGO is initially
537 promoted by a dye-sensitized mechanism. In the presence of rGO, electrons are mostly
538 transferred to rGO, and then from rGO to TiO_2. When excited electrons in rGO cannot be
539 released (for example to TiO_2, for which rGO acts as sensitizer and also as hole acceptor), rGO
540 acts a recombination center.

13

4. Conclusions

The analysis of the photocatalytic behavior of TiO_2-rGO hybrid materials synthesized at different loading of rGO, underlines its complexity as the working mechanisms depend not only on the substrate degraded, but also on the kind of irradiation adopted. A careful optical characterization of the hybrid materials and lamp emission allows disentangling many tricky rate trends observed changing % rGO in the hybrid catalyst. Phenol is degraded predominantly via UV-based photocatalysis and the content of rGO decreases the rate by increasing the amount of scattered light. MB is degraded via UV-based photocatalysis and in the case of visible irradiation via a dye-sensitized mechanism. Visible sensitization driven by rGO phase seems not to be the predominant mechanism in the studied experimental conditions and with the studied photocatalytic materials. However, rGO plays a key role for adsorption and as electron passageway for dye-sensitized mechanism. Because the adsorption of MB on the TiO_2 surfaces activates the dye-sensitized process which is not directly related to the real photocatalytic features of the hybrid material, the studies that use MB alone with hybrid materials and illumination with not well characterized emission could lead to misleading conclusions on the role of rGO. It is not possible to generalize the conclusions obtained on the photocatalytic behavior of the materials we synthesized to the entire set of reported TiO_2-rGO materials, because the numerous modifications of the TiO_2-rGO synthetic strategies can affect abruptly their photocatalytic performance. In particular the degree of rGO reduction can influence the energy position of its LUMO allowing/hindering the electron injection from/toward adsorbed species. Residual oxygenated groups on rGO can also be involved in acid-base equilibria which can shift the Fermi level position of rGO as a function of pH, changing the relative position of its electronic states in comparison with those of TiO_2.

Our study strongly suggests that among many mechanisms reported on the role of rGO (and graphene) the electron transfer process can occur from photoexcited states of rGO onto the titania, and holes from titania migrate to it, where adsorbed substrates are oxidized only if their HOMO has higher energy (less positive standard redox potential) than the empty state of excited rGO. Then, reduced graphene (and possibly also graphene) is advantageous when substrates are adsorbed and when the charge separation is possible (coupled with a proper semiconductor like TiO_2). Alone, or coupled with low work function oxides, rGO could be ineffective.
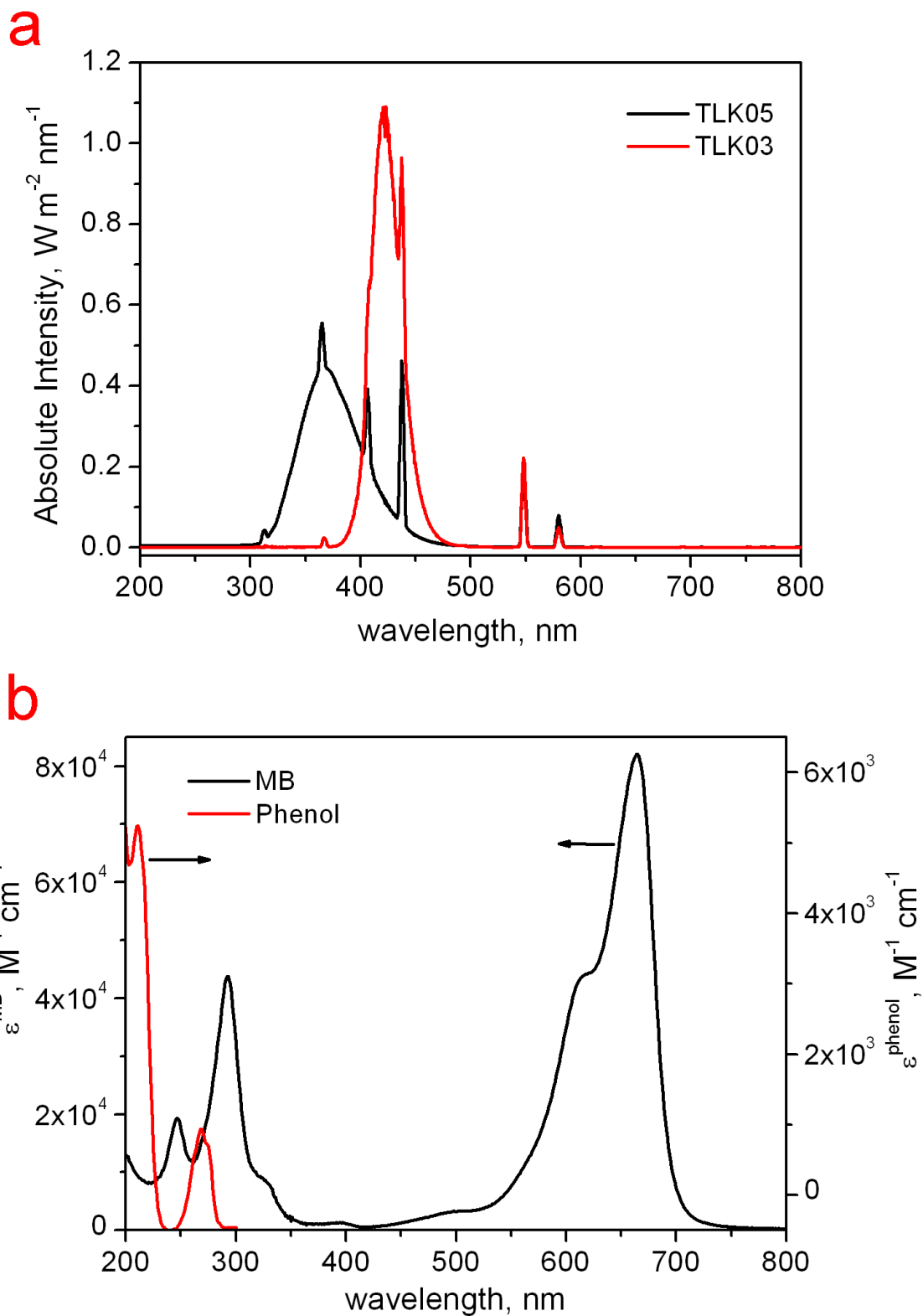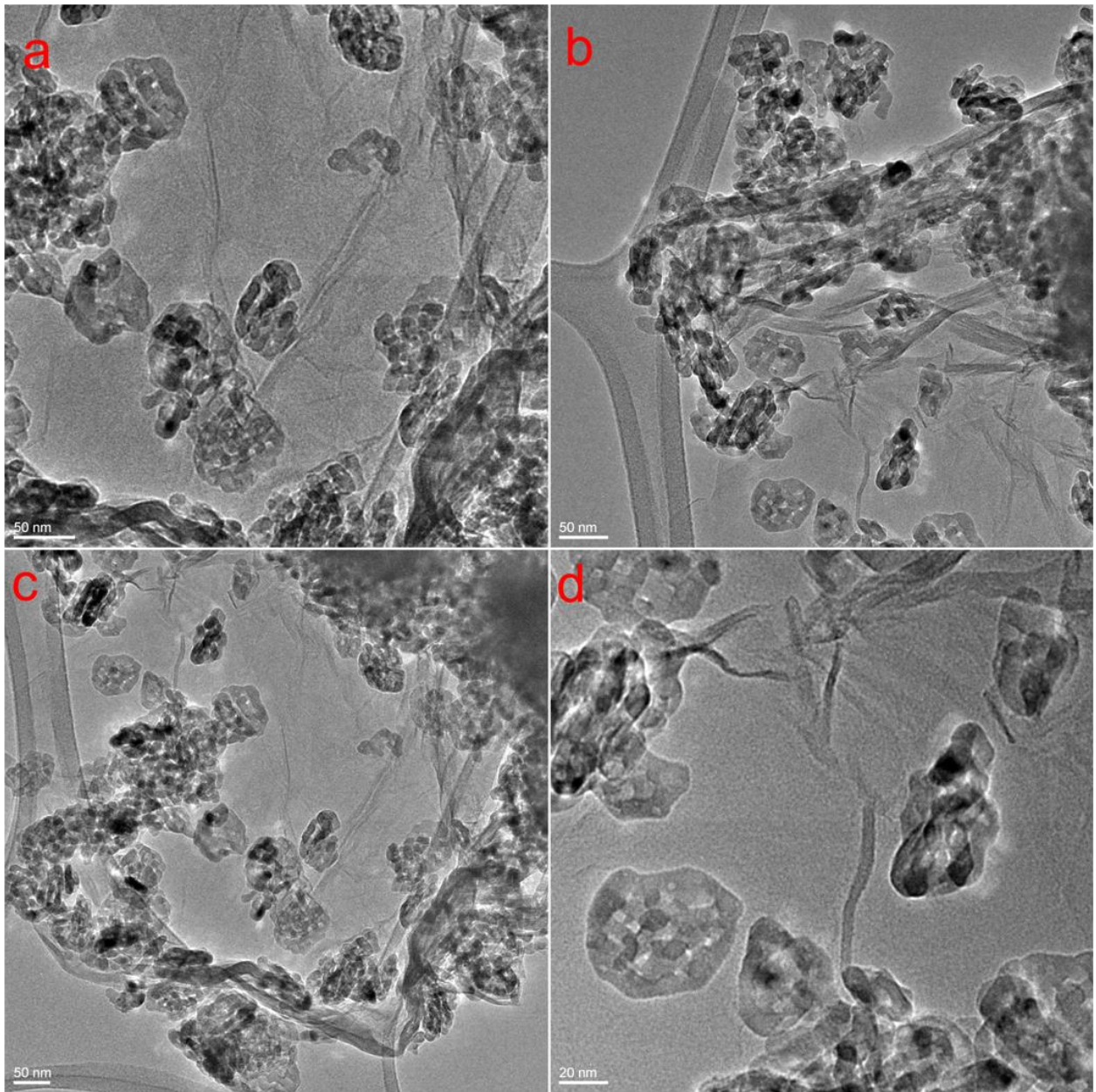
14

SUPPLEMENTARY MATERIAL

583

Fig. 1-SM (A) Emission spectra of the lamps adopted for the irradiation tests in the 200-800 nm range; (B) Absorption spectra of phenol and methylene blue in the 200-800 nm range.
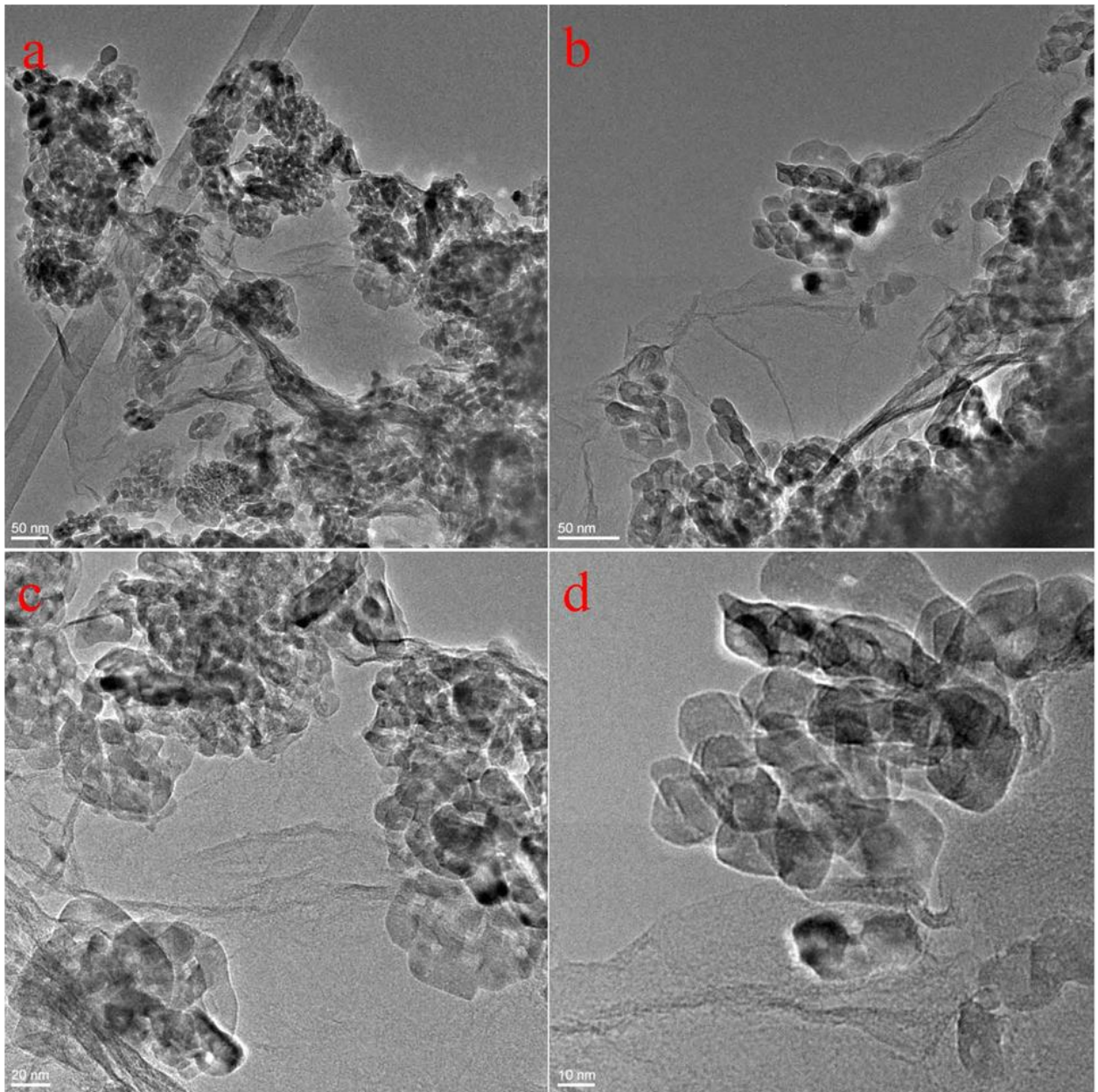
586

Fig. 2-SM HR-TEM micrographs of the sample TiO$_2$-GO before chemical reduction with 5% GO loading. Original magnifications: a) $\times$ 50 k, b) $\times$ 40 k, c) $\times$ 30 k and d) $\times$ 100 k.
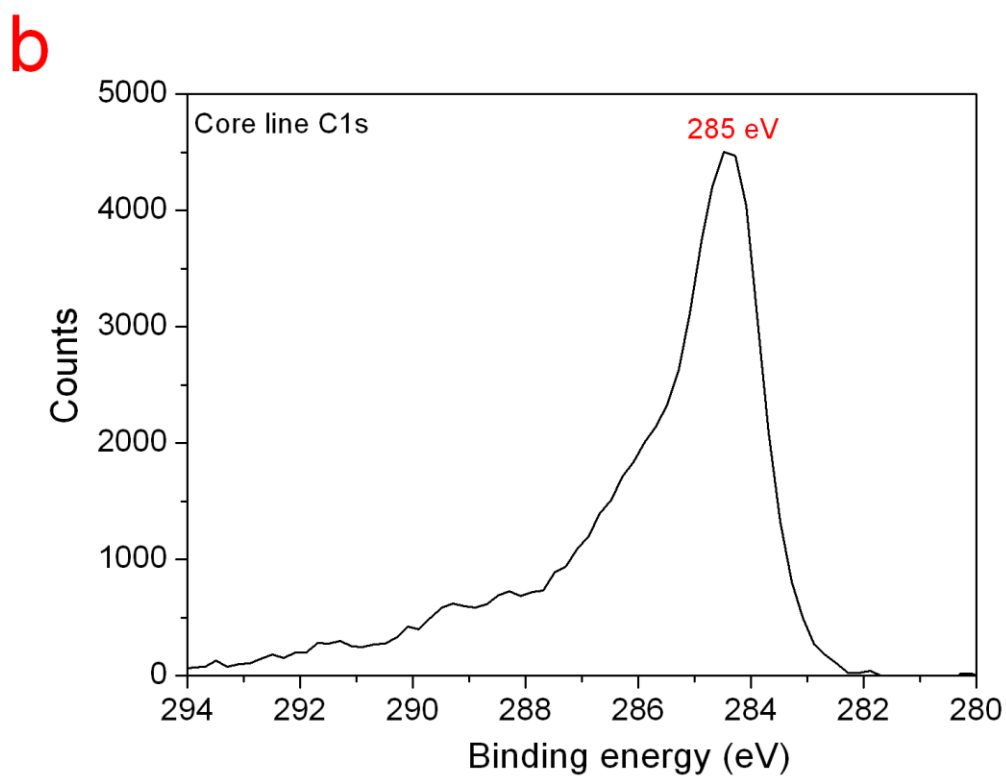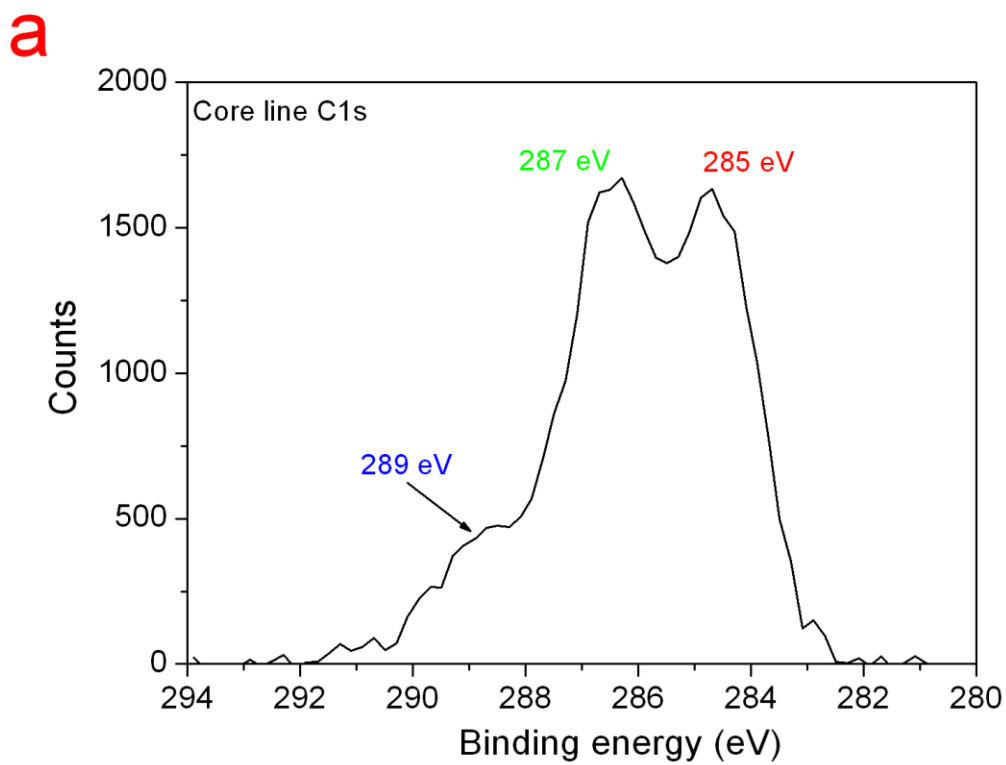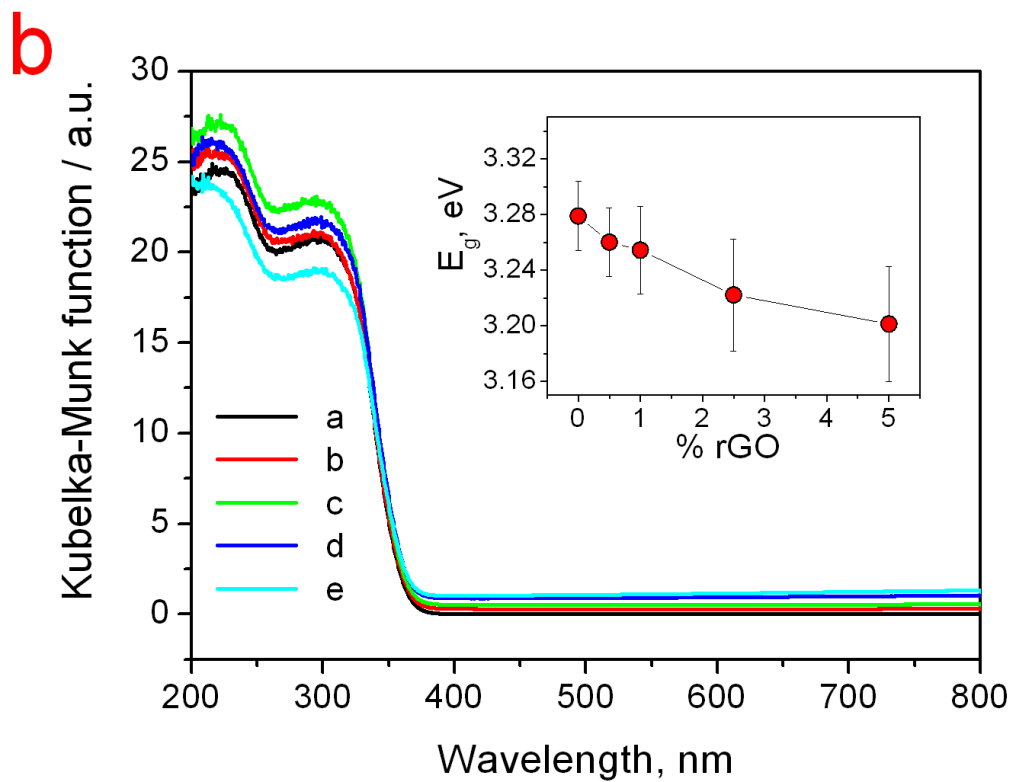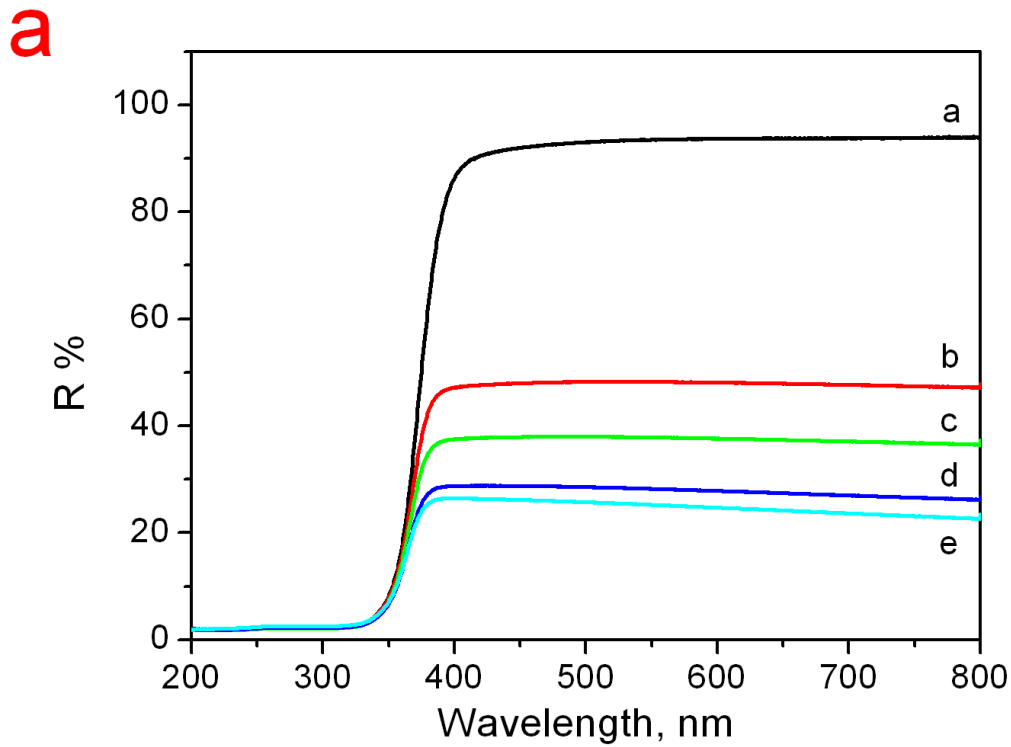
587
588
589
590

591

592
593

Fig. 3-SM (A) HR-TEM micrographs of the sample TiO$_2$-rGO with 5% rGO loading. Original magnifications: a) × 30 k, b) × 40 k, c) × 100 k and d) × 200 k.

596

17

Fig. 4-SM. XPS-ESCA peak of C(1s) core level of a) TiO$_2$- GO, b) TiO$_2$-rGO(chem), with a 5% GO/rGO loading.

18

602
603

Fig. 5-SM Diffuse reflectance spectra of TiO_2-rGO hybrid materials at different rGO loadings: a = 0, b = 0.5, c = 1, d = 2.5 and e = 5 %; A) Spectra in % Reflectance; B) Spectra in Kubelka-Munk function (inset: apparent bang gap as a function of the % rGO.

607

608   **Table 1-SM** Pseudo first-order kinetic constants with the related error for all the photocatalytic
609   transformation of phenol and MB under irradiated (UV-Vis and Vis only)
610

Entry	Substrate	Irradiation	%rGO	k, min^{-1}
1	Phenol	UV-Vis	0	$(4.91\pm0.09)\times10^{-3}$
2	Phenol	UV-Vis	0.5	$(4.0\pm0.1)\times10^{-3}$
3	Phenol	UV-Vis	1	$(3.8\pm0.1)\times10^{-3}$
4	Phenol	UV-Vis	2.5	$(3.20\pm0.07)\times10^{-3}$
5	Phenol	UV-Vis	5	$(2.36\pm0.06)\times10^{-3}$
6	MB	UV-Vis	0	$(3.8\pm0.4)\times10^{-2}$
7	MB	UV-Vis	1	$(2.0\pm0.2)\times10^{-2}$
8	MB	UV-Vis	2.5	$(1.6\pm0.1)\times10^{-2}$
9	MB	UV-Vis	5	$(4.0\pm0.4)\times10^{-2}$
10	MB	Vis only	0	$(1.6\pm0.1)\times10^{-3}$
11	MB	Vis only	1	$(1.29\pm0.05)\times10^{-3}$
12	MB	Vis only	2.5	$(1.75\pm0.12)\times10^{-3}$
13	MB	Vis only	5	$(2.6\pm0.1)\times10^{-3}$

611
612
613
614

615   *References*

[1] M.R. Hoffman, S.T. Martin, W. Choi, D.W. Bahnemann, Chem. Rev. 95 (1995) 69-96.

[2] T.L. Thompson, J.T. Yates, Chem. Rev. 106 (2006) 4428-4453.

[3] C. Minero, V. Maurino, E. Pelizzetti, Mechanism of the Photocatalytic Transformation of Organic Compounds, in: V. Ramamurthy, K.S. Schanze (Eds.), Semiconductor Photochemistry and Photophysics (Molecular and Supramolecular Photochemistry, Vol. 10), Marcel Dekker, New York, 2003, pp. 211-229.

[4] R. Wang, K. Hashimoto, A. Fujishima, Nature 388 (1997) 431-432.

[5] B. O'Regan, M. Grätzel, Nature 353 (1991) 737-739.

[6] V. Maurino, A. Bedini, M. Minella, F. Rubertelli, E. Pelizzetti, C. Minero, J. Adv. Oxid. Technol. 11 (2008) 184-192.

[7] C. Minero, Catal. Today 54 (1999) 205-216.

[8] J.C. Yu, J. Yu, W. Ho, Z. Jiang, L. Zhang, Chem. Mater. 14 (2002) 3808-3816.

[9] G. Barolo, S. Livraghi, M. Chiesa, M.C. Paganini, E. Giamello, J. Phys. Chem. C 116 (2012) 20887-20894.

[10] G. Yang, Z. Yan, T. Xiao, Appl. Surf. Sci. 258 (2012) 8704-8712.

[11] Y. Shiraishi, D. Tsukamoto, Y. Sugano, A. Shiro, S. Ichikawa, S. Tanaka, T. Hirai, ACS Catal. 2 (2012) 1984-1992.

[12] F. Sordello, C. Duca, V. Maurino, C. Minero, Chem. Commun. 47 (2011) 6147-6149.

[13] F. Sordello, V. Maurino, C. Minero, J. Mater. Chem. 21 (2011) 19144-19152.

[14] S. Lou, X. Guo, T. Fan, D. Zhang, Energy Environ. Sci. 5 (2012) 9195-9216.

[15] F. Sordello, C. Minero, Appl. Catal. B: Environ. 163 (2015) 452-458.

[16] C. Minero, G. Mariella, V. Maurino, E. Pelizzetti, Langmuir 16 (2000) 2632-2641.

[17] M. Minella, M.G. Faga, V. Maurino, C. Minero, E. Pelizzetti, S. Coluccia, G. Martra, Langmuir 26 (2010) 2521-2527.

[18] N. Zhang, Y. Zhang, Y.-J. Xu, Nanoscale 4 (2012) 5792-5813.

[19] V.R. Djokić, A.D. Marinković, M. Mitrić, P.S. Uskoković, R.D. Petrović, V.R. Radmilović, D.T. Janaćković, Ceram. Int. 38 (2012) 6123-6129.

[20] S. Battiston, M. Minella, R. Gerbasi, F. Visentin, P. Guerriero, A. Leto, G. Pezzotti, E. Miorin, M. Fabrizio, C. Pagura, Carbon 48 (2010) 2470-2477.

[21] L.-L. Tan, S.-P. Chai, A.R. Mohamed, ChemSusChem 5 (2012) 1868-1882, and references therein.

[22] K.S. Novoselov, A.K. Geim, S.V. Morozov, D. Jiang, Y. Zhang, S.V. Dubonos, I.V. Grigorieva, A.A. Firsov, Science 306 (2004) 666-669.

[23] J.N. Coleman, M. Lotya, A. O'Neill, S.D. Bergin, P.J. King, U. Khan, K. Young, A. Gaucher, S. De, R.J. Smith, I.V. Shvets, S.K. Arora, G. Stanton, H.-Y. Kim, K. Lee, G.T. Kim, G.S. Duesberg, T. Hallam, J.J. Boland, J.J. Wang, J.F. Donegan1, J.C. Grunlan, G. Moriarty, A. Shmeliov, R.J. Nicholls, J.M. Perkins, E.M. Grieveson, K. Theuwissen, D.W. McComb, P.D. Nellist, V. Nicolosi, Science 331 (2011) 568-571.

[24] C. Berger, Z. Song, X. Li, X. Wu, N. Brown, C. Naud, D. Mayou, T. Li, J. Hass, A.N. Marchenkov, E.H. Conrad, P.N. First, W.A. de Heer, Science 312 (2006) 1191-1196.

[25] M. Peplow, Nature 503 (2013) 327-329.

[26] L. Anfossi, P. Calza, F. Sordello, C. Giovannoli, F. Di Nardo, C. Passini, M. Cerruti, I.Y. Goryacheva, E.S. Speranskaya, C. Baggiani, Anal. Bioanal. Chem. 406 (2014) 4841-4849.

[27] F. Sordello, G. Zeb, K. Hu, P. Calza, C. Minero, T. Szkopekc, M. Cerruti, Nanoscale, 6 (2014) 6710-6719.

[28] T. Szabó, O. Berkesi, P. Forgó, K. Josepovits, Y. Sanakis, D. Petridis, I. Dékány, Chem. Mater. 18 (2006) 2740-2749.

[29] M. Minella, M. Demontis, M. Sarro, F. Sordello, P. Calza, C. Minero, J. Mater. Sci. 50 (2015) 2399-2409.

21

[30] L.M. Pastrana-Martínez, S. Morales-Torres, V. Likodimos, J.L. Figueiredo, J.L. Faria, P. Falaras, A.M.T. Silva, Appl. Catal. B: Environ. 123-124 (2012) 241-256.

[31] Y. Wang, R. Shi, J. Lin, Y. Zhu, Appl. Catal. B: Environ. 100 (2010) 179-183.

[32] R. Long, N.J. English, O.V. Prezhdo, J. Am. Chem. Soc. 134 (2012) 14238-14248.

[33] Y. Zhang, N. Zhang, Z.-R. Tang, Y.-L. Xu, ACS Nano 6 (2012) 9777-9789.

[34] G. Williams, B. Seger, P.V. Kamat, ACS Nano 2 (2008) 1487-1491.

[35] I.V. Lightcap, T.H. Kosel, P.V. Kamat, Nano Lett. 10 (2010) 577-583.

[36] J. Zhang, Z. Xiong, X.S. Zhao, J. Mater. Chem. 21 (2011) 3634-3640.

[37] P. Wang, J. Wang, X. Wang, H. Yu, J. Yu, M. Lei, Y. Wang, Appl. Catal. B: Environ. 132-133 (2013) 452-459.

[38] E. Pelizzetti, V. Maurino, C. Minero, V. Carlin, E. Pramauro, O. Zerbinati, Environ Sci Technol 24 (1990) 1559-1565.

[39] V. Maurino, M. Minella, F. Sordello, C. Minero, Appl. Catal. A: Gen. (2015) http://dx.doi.org/10.1016/j.apcata.2015.11.012.

[40] W.S. Hummers, R.E. Offeman, J. Am. Chem. Soc. 80 (1958) 1339.

[41] N.M. Huang, H.N. Lim, C.H. Chia, M.A. Yarmo, M.R. Muhamad, Int. J. Nanomed. 6 (2011) 3443-3448.

[42] W. Fan, Q. Lai, Q. Zhang, Y. Wang. J. Phys. Chem. C 115 (2011) 10694-10701.

[43] V. Pagonis, C. Ankjærgaard, A.S. Murray, R. Chen, J. Lumin. 129 (2009) 1003-1009.

[44] M. Lotya, Y. Hernandez, P.J. King, R.J. Smith, V. Nicolosi, L.S. Karlsson, F.M. Blighe, S. De, Z. Wang, I.T. McGovern, G.S. Duesberg, J.N. Coleman, J. Am. Chem. Soc. 131 (2009) 3611-3620.

[45] A.B. Bourlinos, V. Georgakilas, R. Zboril, T.A. Steriotis, A.K. Stubos, C. Trapalis, Solid State Commun. 149 (2009) 2172-2176.

[46] Q. Mei, K. Zhang, G. Guan, B. Liu, S. Wang, Z. Zhang, Chem. Commun. 46 (2010) 7319-7321.

[47] D. Li, M.B. Mueller, S. Gilje, R.B. Kaner, G.G. Wallace, Nat. Nanotechnol. 3 (2008) 101-105.

[48] D.C. Marcano, D.V. Kosynkin, J.M. Berlin, A. Sinitskii, Z. Sun, A. Slesarev, L.B. Alemany, W. Lu, J.M. Tour, ACS Nano 4 (2010) 4806-4814.

[49] X. Gao, J. Jang, S. Nagase, J. Phys. Chem. C 114 (2010) 832-842.

[50] N. M. Huang, H. N. Lim, C. H. Chia, M. A. Yarmo, M. R. Muhamad, Int. J. Nanomed. 6 (2011) 3443-3448.

[51] S. Pei, H.-M. Cheng, Carbon 50 (2012) 3210-3228

[52] M. Bruna, B. Massessi, C. Cassiago, A. Battiato, E. Vittone, G. Speranza, S. Borini, J. Mater. Chem. 51 (2011) 18730-18737.

[53] J. Shang, L. Ma, J. Li, W. Ai, T. Yu, G.G. Gurzadyan, Sci. Rep. 2 (2012) 792, DOI: 10.1038/srep00792.

[54] Y. Zhang, Z.-R. Tang, X. Fu, Y.-J. Xu, ACS Nano 4 (2010) 7303-7314.

[55] H. Zhang, X. Lv, Y. Li, Y. Wang, J. Li, ACS Nano 4 (2010) 380-386.

[56] V. Štengl, D. Popelková, P. Vláčil, J. Phys. Chem. C 115 (2011) 25209-25218.

[57] K. Woan, G. Pyrgiotakis, W. Sigmund, Adv. Mater. 21 (2009) 2233-2239.

[58] M.S.A.S. Shah, A.R. Park, K. Zhang, J.H. Park, P.J. Yoo, Appl. Mater. Interfaces 4 (2012) 3893-3901.

[59] B. El-Kareh, Fundamentals of Semiconductor Processing Technologies, Kluwer Academic Publishers, Norwell, 1995.

[60] M. Liška, Ľ. Bartoš, J. Valášek, Chem. Papers 43 (1989) 303-313, and references therein.

[61] K. Patil, R. Pawar, P. Talap, Phys. Chem. Chem. Phys. 2 (2000) 4313-4317.

[62] A. Ghanadzadeh, A. Zeini, A. Kashef, M. Moghadam, J. Mol. Liq. 138 (2008) 100-106.

[63] T. Xiong, F. Dong, Y. Zhou, M. Fu, W.-K. Ho, J. Colloid. Interface Sci. 447 (2015) 16-24.

22

[64] P. Calza, C. Hadjicostas, V.A. Sakkas, M. Sarro, C. Minero, C. Medana, T.A. Albanis, Appl. Catal. B: Environ. 183 (2016) 96-106.

[65] N. Martsinovich, A. Troisi, Phys. Chem. Chem. Phys. 14 (2012) 13392-13401.

[66] R. Abe, K. Sayama, H. Arakawa, J. Photochem. Photobiol., A 166 (2004) 115-122.

[67] M.-Q. Yang, Y.-J. Xu, J. Phys. Chem. C 117 (2013) 21724−21734.

23